PERGAMON

International Journal of Solids and Structures 36 (1999) 4699–4723

INTERNATIONAL JOURNAL OF SOLIDS and STRUCTURES

Space-time finite elements for the analysis of transient wave propagation in unbounded layered media

M.N. Guddati[a], J.L. Tassoulas[b,*]

[a] *Texas Institute for Computational and Applied Mathematics, The University of Texas at Austin, Austin, TX 78712-1076, U.S.A.*

[b] *Department of Civil Engineering, The University of Texas at Austin, Austin, TX 78712-1076, U.S.A.*

Received 24 May 1997; accepted 6 October 1997

Abstract

A new method is proposed for the analysis of transient wave propagation in a layered stratum. It makes use of the separation of variables technique and reduces the spatial dimension of analysis to one. The resulting system of hyperbolic partial differential equations is solved via element-by-element computations based on a space-time Galerkin finite element method. This method is shown to be more efficient than the methods based on convolution. Numerical examples are presented to illustrate the effectiveness of the method. Current limitations and possible extensions are also discussed.

Keywords: Soil–structure interaction; Fluid–structure interaction; Transmitting boundaries; Absorbing boundaries; Unbounded domains; Wave propagation

1. Introduction

Analysis of unbounded media for arbitrary types of dynamic loading is of prime interest in many fields of engineering such as acoustics, soil-structure interaction and fluid-structure interaction. The special case of modeling unbounded layers arises in soil–structure interaction and dam–reservoir interaction problems. Soil is generally modeled as a stratified elastic layer resting on rock. In dam–reservoir problems, the fluid is modeled as an acoustic layer fixed at the bottom. The aim of these analyses is the response of a structure embedded in the infinite medium.

The standard way of analyzing problems of this type (Fig. 1) is to truncate the unbounded medium in order to render the computational domain finite and apply absorbing boundary conditions at the computational boundary. The resulting bounded domain can be analyzed using a standard finite element method. Several ways of obtaining the boundary conditions to simulate

* Corresponding author

0020-7683/99/$ - see front matter
PII: S0020-7683(98)00261-3

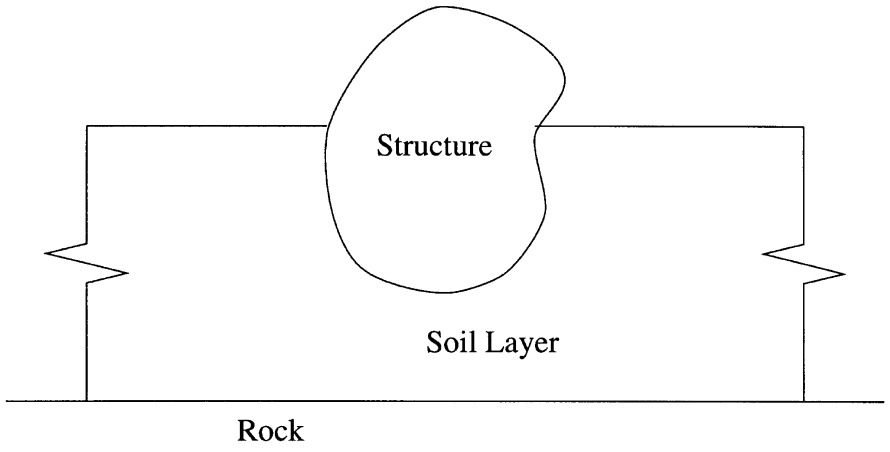

(a) Physical Problem

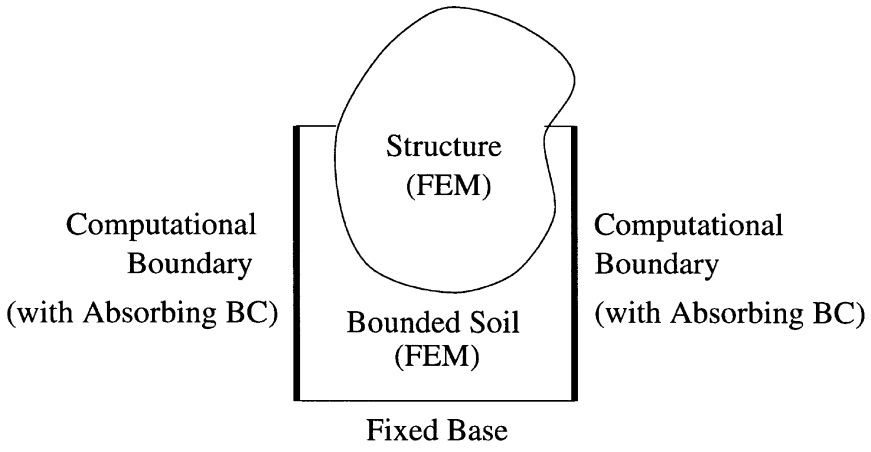

(b) Mathematical Model

Fig. 1. General method of analysis for unbounded media.

the unbounded medium have been suggested (see Givoli, 1992 for a review). These boundary conditions can be classified into two broad categories: local and global. Local boundary conditions involve derivatives of the field variables with respect to space and time and result in an economical numerical procedure. However, their performance is limited to narrow ranges of wavelength along the computational boundary. On the other hand, global boundary conditions are highly accurate in modeling infinite media. They are, however, very expensive due to full coupling in space and time.

The main focus in the direction of global methods has been on obtaining the impulse response function of the exterior domain. The impulse response function is used in conjunction with convolution to analyze the effect of unbounded media. Impulse response functions can be obtained using several techniques (Kausel, 1992), including Fourier transformation of the dynamic stiffness matrix of the unbounded medium from the frequency domain to the time domain. The frequency-domain stiffness matrix can be computed using the methods of Waas (1972), Kausel et al. (1975), Tassoulas (1981) and Lin and Tassoulas (1986). These methods result in what have become known as consistent transmitting boundaries and are based on separation of variables and semi-discretization. Another way of obtaining the frequency-domain stiffness is the use of cloning suggested by Roesset and Scaletti (1979) and Dasgupta (1982). Their methods make use of similarity and dynamic condensation to obtain the approximate dynamic stiffness matrix for the unbounded media. Recently, this idea was extended by Wolf and Song (1996) to obtain the Consistent Infinitesimal Finite Element Cell Method. This method is a clever use of similarity and suggests a way of obtaining the impulse response function without resorting to Fourier transforms. However, the method requires expensive computations such as solution of a matrix Ricatti equation and solution of a linear equation of type $AX+XA+tX=B$ (A and B are known matrices, t is a known scalar and X is the matrix to be determined). These convolution-based methods seem demanding, even with some attractive recursive techniques suggested by Wolf (1988).

With the objective of obtaining a more economical global method, we take a new direction of solving the governing equations in the space-time domain. Two main steps involved in these methods are the use of semidiscretization to reduce the spatial dimension to one and the solution of the resulting system of hyperbolic partial differential equations in an efficient manner. The case of a homogeneous acoustic layer has been successfully tackled by the use of a characteristics method (see Guddati and Tassoulas, 1997a). The extension of the method to more general geometries is presented in Guddati and Tassoulas (1997b). Although the characteristics method is highly efficient compared to all the existing methods, an equally efficient extension to the case of layered media does not seem likely. In this paper, we present a new space-time Galerkin technique for the analysis of transient wave propagation in unbounded layered media. The method is based on the concept of domain of determinacy and leads to element-by-element computations.

The outline of the paper is as follows: Section 2 discusses the preliminaries and states precisely the problems to be solved. In Section 3, semidiscretization is discussed, while Section 4 is devoted to the new space-time Galerkin (STG) procedure. Section 5 deals with the computational cost of the proposed method. In Section 6, numerical examples are presented to evaluate the effectiveness of the method. The final section contains a brief summary, current limitations and possible extensions.

2. Problem statement

Waves described by linear second-order hyperbolic partial differential equations occur in several fields including acoustics, elasticity and electromagnetics. In this section, we state the typical wave equations of interest and precisely formulate the continuous problems to be solved. The wave propagation in linearly elastic media is represented by the following vector wave equation (see Achenbach, 1973; Bedford and Drumheller, 1994).

$$\rho\frac{\partial^2\mathbf{u}}{\partial t^2}-\nabla((\lambda+2G)\nabla\cdot\mathbf{u})+\nabla\times(G\nabla\times\mathbf{u})=\mathbf{f}, \tag{1}$$

where $\mathbf{u}$ is the displacement vector, ρ is the density, λ and G are Lamé constants and $\mathbf{f}$ is the body force vector. When the above equation is restricted to two-dimensions, we get the governing equation for wave propagation under plane strain. In the case of antiplane shear, the vector wave equation is reduced to the following scalar wave equation:

$$\rho\frac{\partial^2 u}{\partial t^2}-\nabla\cdot(G\nabla u)=f. \tag{2}$$

A similar scalar wave equation represents wave propagation in acoustic media.

It is our aim to simulate the infinite layered media governed by differential equations of the form of eqns (1) and (2). We assume the computational boundary Γ to be a straight edge perpendicular to the layer. Dirichlet conditions are applied at the bottom and Neumann conditions are applied on the top. The layer is assumed to start from rest. The material constants do not vary in the horizontal direction, but can vary in the vertical direction. The problem setting is clearly shown in Fig. 2. For reasons that will be apparent later, we write the statement of the initial-boundary-value problem in terms of the specific coordinate system of the layer. Then, the scalar wave problem takes the following form.

Problem CLayer: Find the (Dirichlet-to-Neumann) map $DtN: u_\Gamma \to s$ in which u_Γ is the field variable at the boundary ($x=0$) and $s=-Gu_x$ is the traction on the boundary. The field variable satisfies the following differential equation, boundary conditions and initial conditions:

$$\rho u_{tt}-Gu_{xx}-(Gu_z)_z=f \quad \text{for } x>0, \quad z\in(-H,0), \quad t>0, \tag{3}$$

$$u(x,z,t)=\bar{u}(x,t) \qquad \text{at } z=-H, \tag{4}$$

$$Gu_z(x,z,t)=\bar{s}(x,t) \qquad \text{at } z=0, \tag{5}$$

$$u(x,z,0)=u_t(x,z,0)=0. \tag{6}$$

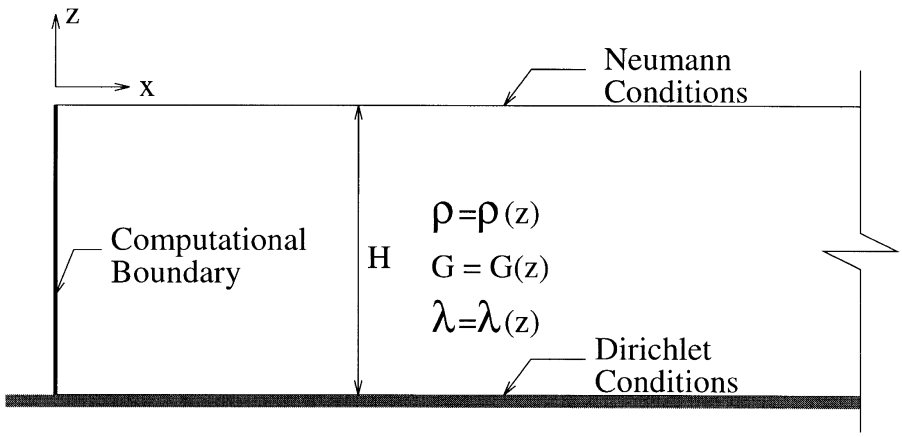

Fig. 2. Wave propagation in semi-infinite layered media.

In the case of elastic wave propagation problems, the boundary conditions can be specified in terms of displacements ($\mathbf{u} = \bar{\mathbf{u}}$) and/or tractions ($\sigma \cdot \mathbf{n} = \bar{\mathbf{s}}$). The DtN map should relate the tractions with the displacements. In the specific case of a layer (Fig. 2), the traction on the interaction boundary is given by:

$$\mathbf{s} = -\begin{bmatrix} \lambda+2G & \\ & G \end{bmatrix}\frac{\partial \mathbf{u}}{\partial x} - \begin{bmatrix} & \lambda \\ G & \end{bmatrix}\frac{\partial \mathbf{u}}{\partial z}. \tag{7}$$

The elastic wave propagation problem then takes the following form.

Problem CLayerE: Find the map $DtN: \mathbf{u}_\Gamma \to \mathbf{s}$ in which $\mathbf{u}_\Gamma$ is the field variable at the boundary ($x = 0$) and $\mathbf{s}$, defined by eqn (7), is the traction on the boundary. The field variable satisfies the following differential equation, boundary conditions and initial conditions:

$$\begin{bmatrix} \rho & \\ & \rho \end{bmatrix}\frac{\partial^2 \mathbf{u}}{\partial t^2} - \begin{bmatrix} \lambda+2G & \\ & G \end{bmatrix}\frac{\partial^2 \mathbf{u}}{\partial x^2} - \frac{\partial}{\partial z}\left(\begin{bmatrix} G & \\ & \lambda+2G \end{bmatrix}\frac{\partial \mathbf{u}}{\partial z}\right) - \frac{\partial}{\partial x}\left(\begin{bmatrix} & \lambda \\ G & \end{bmatrix}\frac{\partial \mathbf{u}}{\partial z}\right) - \frac{\partial}{\partial z}\left(\begin{bmatrix} & G \\ \lambda & \end{bmatrix}\frac{\partial \mathbf{u}}{\partial x}\right) = \mathbf{f} \quad \text{for} \quad \begin{matrix} x > 0, \\ z \in (-H, 0), \\ t > 0 \end{matrix} \tag{8}$$

$$\mathbf{u}(x, z, t) = \bar{\mathbf{u}}(x, t) \quad \text{at } z = -H \tag{9}$$

$$\begin{bmatrix} & G \\ \lambda & \end{bmatrix}\frac{\partial \mathbf{u}}{\partial x} + \begin{bmatrix} G & \\ & \lambda+2G \end{bmatrix}\frac{\partial \mathbf{u}}{\partial z} = \bar{\mathbf{s}}(x, t) \quad \text{at } z = 0 \tag{10}$$

$$\mathbf{u}(x, z, 0) = \mathbf{u}_t(x, z, 0) = 0. \tag{11}$$

3. Semidiscretization

In this section, the first level of approximation is performed: the boundary is discretized to reduce the spatial dimension of the problem to one. This is facilitated by the special geometry of the unbounded domain. The method is explained in detail for the scalar wave equation and the semidiscrete counterparts for the elastic wave equation are presented.

3.1. Scalar wave equation

The following approximation is used for the displacement field:

$$u_h = \sum_{i=1}^{N} \phi_i(z) u_i(x, t) = \mathbf{\Phi}^T(z)\mathbf{U}(x, t). \tag{12}$$

In the above, $\mathbf{\Phi}(z)$ can be viewed as the basis function vector in the z-direction and $\mathbf{U}(x, t)$ is the vector of nodal degrees of freedom.

We apply the standard Galerkin method using this approximation. The test function is of the same form as the solution:

$$\delta u_h = \sum_{i=1}^{N} \phi_i(z)\delta u_i(x,t) = \mathbf{\Phi}^T(z)\delta\mathbf{U}(x,t). \tag{13}$$

We get the Galerkin approximation of the variational form of the original equation as

$$\int_{z=-H}^{z=0} \delta u_h(Gu_{xx} + (Gu_z)_z - \rho u_{tt} + f)\,\mathrm{d}z = 0. \tag{14}$$

Integrating by parts with respect to z, we get

$$-\int_{-H}^{0} \frac{\partial \delta u_h}{\partial z} G \frac{\partial u_h}{\partial z}\,\mathrm{d}z + \int_{-H}^{0} \delta u_h G \frac{\partial^2 u_h}{\partial x^2}\,\mathrm{d}z - \int_{-H}^{0} \delta u_h \rho \frac{\partial^2 u_h}{\partial t^2}\,\mathrm{d}z + \int_{-H}^{0} \delta u_h f\,\mathrm{d}z = 0. \tag{15}$$

Substituting the approximation for u_h gives rise to

$$-\delta\mathbf{U}^T \int_{-H}^{0} G\mathbf{\Phi}_z\mathbf{\Phi}_z^T\,\mathrm{d}z\mathbf{U} + \delta\mathbf{U}^T \int_{-H}^{0} G\mathbf{\Phi}\mathbf{\Phi}^T\,\mathrm{d}z\mathbf{U}_{xx} - \delta\mathbf{U}^T \int_{-H}^{0} \rho\mathbf{\Phi}\mathbf{\Phi}^T\,\mathrm{d}z\mathbf{U}_{tt} + \delta\mathbf{U}^T \int_{-H}^{0} \mathbf{\Phi} f\,\mathrm{d}z + G\delta\mathbf{U}^T\mathbf{\Phi}|_{z=0}s_0 = 0, \tag{16}$$

which can be written in the following form:

$$-\mathbf{G}\mathbf{U} + \mathbf{A}\mathbf{U}_{xx} - \mathbf{M}\mathbf{U}_{tt} + \mathbf{F} = 0. \tag{17}$$

In the above $\mathbf{G}$, $\mathbf{A}$ and $\mathbf{M}$ are constant $N \times N$ matrices and $\mathbf{F}$ is a vector function of x and t:

$$\mathbf{G} = \int_{-H}^{0} \mathbf{\Phi}_z G \mathbf{\Phi}_z^T\,\mathrm{d}z, \tag{18}$$

$$\mathbf{A} = \int_{-H}^{0} \mathbf{\Phi} G \mathbf{\Phi}^T\,\mathrm{d}z, \tag{19}$$

$$\mathbf{M} = \int_{-H}^{0} \mathbf{\Phi}\rho\mathbf{\Phi}^T\,\mathrm{d}z, \tag{20}$$

$$\mathbf{F}(x,t) = \int_{-H}^{0} \mathbf{\Phi} f\,\mathrm{d}z + G\mathbf{\Phi}|_{z=0}s_0. \tag{21}$$

Note that the matrices $\mathbf{A}$ and $\mathbf{M}$ are of Grammian type, and thus positive definite. Matrix $\mathbf{G}$ is positive semidefinite, in general, and is positive definite when Dirichlet conditions are applied on one or both of the surfaces.

Our modified problem is to find a map between the displacement vector $\mathbf{U}_\Gamma$ and the traction vector consistent with the approximation made in displacement, i.e. if $\mathbf{S}$ is the traction vector, we need to satisfy the variational equivalence:

$$\delta \mathbf{U}^T \mathbf{S} = \int_{-H}^{0} \delta u_h s_h \, \mathrm{d}z, \tag{22}$$

where s_h is the approximation of the traction s. As $s = -Gu_x$, we have $s_h = -\mathbf{\Phi}^T G \mathbf{U}_x$. This results in the following relation:

$$\delta \mathbf{U}^T \mathbf{S} = -\delta \mathbf{U}^T \int_{-H}^{0} \mathbf{\Phi} G \mathbf{\Phi}^T \, \mathrm{d}z \mathbf{U}_x \; \forall \delta \mathbf{U} \in \mathscr{R}^N. \tag{23}$$

This implies, using eqn (19) that the traction vector is nothing but

$$\mathbf{S} = -\mathbf{A}\mathbf{U}_x. \tag{24}$$

We now present the discrete version of our original problem.

Problem DLayer: Find the map $\mathbf{DtN} : \mathbf{U}_\Gamma(t) \to \mathbf{S}(t)$ where $\mathbf{U}_\Gamma$ is the displacement vector at $x = 0$ and $\mathbf{S} = -\mathbf{A}\mathbf{U}_x$ is the corresponding traction vector. We satisfy the following differential equations and initial conditions:

$$\mathbf{A}\mathbf{U}_{xx} - \mathbf{M}\mathbf{U}_{tt} - \mathbf{G}\mathbf{U} + \mathbf{F} = \mathbf{0} \quad \text{for } x > 0, \quad t > 0 \tag{25}$$

$$\mathbf{U} = \mathbf{U}_t = \mathbf{0} \quad \text{at } t = 0. \tag{26}$$

In the above, $\mathbf{A}$ and $\mathbf{M}$ are symmetric positive definite and $\mathbf{G}$ is symmetric positive semidefinite.

3.2. Elastic wave equation

The following approximation is used for the displacement field:

$$\mathbf{u_h} = \sum_{i=1}^{N} \phi_i(z) \mathbf{u_i}(x, t) = \begin{bmatrix} \mathbf{\Phi}^T(z) & & \\ & \ddots & \\ & & \mathbf{\Phi}^T(z) \end{bmatrix} \mathbf{U}(x, t). \tag{27}$$

To facilitate the presentation, we define the following matrix functions:

$$\mathbf{m}(\alpha) = \int_{z=-H}^{z=0} \mathbf{\Phi}^T \alpha(z) \mathbf{\Phi} \, \mathrm{d}z \tag{28}$$

$$\mathbf{g}(\alpha) = \int_{z=-H}^{z=0} \mathbf{\Phi}_z^T \alpha(z) \mathbf{\Phi}_z \, \mathrm{d}z \tag{29}$$

$$\mathbf{d}(\alpha) = \int_{z=-H}^{z=0} \mathbf{\Phi}^T \alpha(z) \mathbf{\Phi}_z \, \mathrm{d}z. \tag{30}$$

Using the above notation, the coefficient matrices arising in the Galerkin approximation are:

$$\mathbf{M} = \begin{bmatrix} \mathbf{m}(\rho) & & \\ & \ddots & \\ & & \mathbf{m}(\rho) \end{bmatrix} \tag{31}$$

$$\mathbf{A} = \begin{bmatrix} \mathbf{m}(\lambda+2G) & \\ & \mathbf{m}(G) \end{bmatrix} \tag{32}$$

$$\mathbf{G} = \begin{bmatrix} \mathbf{g}(G) & \\ & \mathbf{g}(\lambda+2G) \end{bmatrix} \tag{33}$$

$$\mathbf{D} = \begin{bmatrix} & \mathbf{d}(G) \\ \mathbf{d}(\lambda) & \end{bmatrix}. \tag{34}$$

Since $\mathbf{m}(\alpha)$ is symmetric and positive definite for positive α, $\mathbf{M}$ and $\mathbf{A}$ are symmetric positive definite matrices. Similar arguments imply that $\mathbf{G}$ is positive semidefinite. Following a more cumbersome procedure than the one followed for the scalar wave equation, we arrive at the following discrete counterpart for Problem CLayerE.

Problem DLayerE: Find the map $\mathbf{DtN}: \mathbf{U}_\Gamma(t) \to \mathbf{S}(t)$ where $\mathbf{U}_\Gamma$ is the displacement vector at $x = 0$ and $\mathbf{S}$ is the corresponding traction vector given by:

$$\mathbf{S} = \mathbf{A}\mathbf{U}_x + \mathbf{D}\mathbf{U}. \tag{35}$$

The following are the governing differential equations and initial conditions:

$$\mathbf{A}\mathbf{U}_{xx} + (\mathbf{D} - \mathbf{D}^T)\mathbf{U}_x - \mathbf{M}\mathbf{U}_{tt}, -\mathbf{G}\mathbf{U} + \mathbf{F} = \mathbf{0} \quad \text{for } x > 0, \quad t > 0 \tag{36}$$

$$\mathbf{U} = \mathbf{U}_t = \mathbf{0} \quad \text{at } t = 0, \tag{37}$$

where, matrices $\mathbf{A}$ and $\mathbf{M}$ are symmetric positive definite and $\mathbf{G}$ is symmetric positive semidefinite.

We note that problem DLayer is similar to problem DLayerE if we choose $\mathbf{D} = \mathbf{0}$. In the next section we present a method to solve DLayerE using a space-time Galerkin (STG) technique.

4. Space-time Galerkin method

The method presented here is based on the concept of domain of determinacy which is classical in the theory of second-order hyperbolic equations (see Courant and Hilbert, 1966; Garabedian, 1964). For any given curve in space-time with Cauchy data (field variable and normal derivative) specified on it, the domain of determinacy is defined by the region in space-time to which the function can be extended uniquely. The basic idea of the method is as follows. We have a differential equation of the following form:

$$\mathbf{A}\mathbf{U}_{xx} - \mathbf{M}\mathbf{U}_{tt} + (\mathbf{D}^T - \mathbf{D})\mathbf{U}_x - \mathbf{R}\mathbf{U} = 0, \tag{38}$$

where, $\mathbf{A}$ and $\mathbf{M}$ are symmetric and positive definite, and $\mathbf{R}$ is positive semidefinite. We take the spectral decomposition of $\mathbf{A}$ with respect to $\mathbf{M}$, i.e. $\mathbf{M} = \mathbf{Q}\mathbf{Q}^{\mathrm{T}}$ and $\mathbf{A} = \mathbf{Q}\mathbf{\Lambda}\mathbf{Q}^T$. $\mathbf{\Lambda}$ is a diagonal matrix of eigenvalues which are all positive. $\mathbf{Q}$ is the matrix containing all the eigenvectors. Then, the differential equation takes the following form:

$$\mathbf{\Lambda}\hat{\mathbf{U}}_{xx} - \hat{\mathbf{U}}_{tt} + (\hat{\mathbf{D}}^T - \hat{\mathbf{D}})\hat{\mathbf{U}}_x - \hat{\mathbf{R}}\hat{\mathbf{U}} = 0, \tag{39}$$

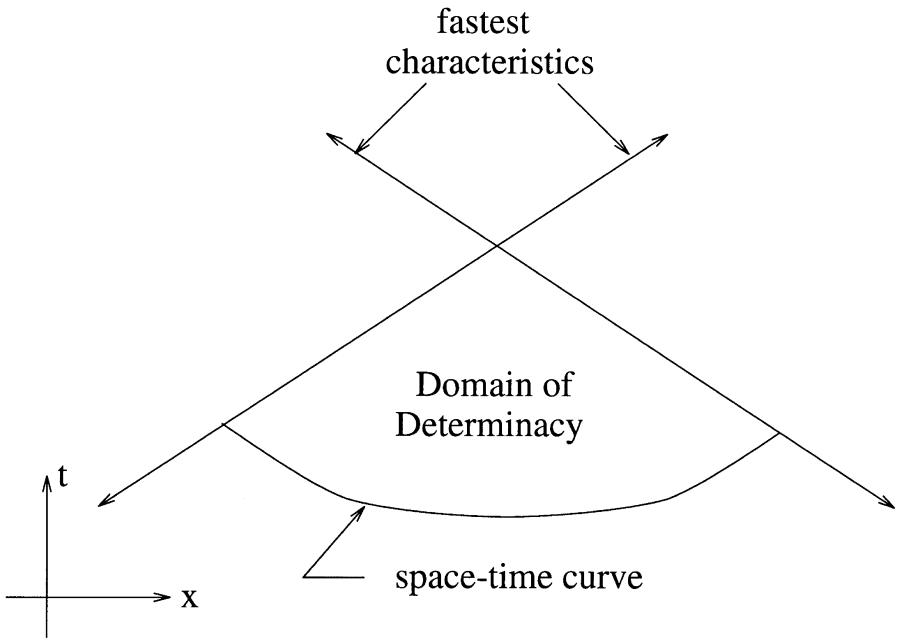

Fig. 3. Domain of determinacy of a curve segment in space time.

where, $\hat{\mathbf{U}} = \mathbf{Q}^T\mathbf{U}$. Note that the eigenvalues (λ_i) are squares of the corresponding horizontal phase velocities of different modes. Thus the fastest speed is given by:

$$c = \sqrt{\lambda_{\max}}, \tag{40}$$

where $\lambda_{\max}$ is the largest eigenvalue of $\mathbf{A}$ with respect to $\mathbf{M}$. Now, the domain of determinacy of a curve segment in space time for this system is the domain bounded by the two fastest characteristics (Fig. 3). In other words, the information (Cauchy data) can not travel faster than the highest phase velocity. Keeping this in mind, we construct a mesh in $x-t$ space which will facilitate element-by-element computation (Fig. 4). The slanted lines in the figure correspond to the highest-speed characteristics.

The procedure is as follows. We know the value of the field variable on the line bounding the mesh on the right ($x-ct=0$). This is because the field variable is not affected by the forcing in the interior. Physically speaking, the effect of the interior is not felt beyond the wavefront. The task is now reduced to solving for $\mathbf{U}$ on the mesh. For the nth time step in the interior (which corresponds to the nth time slab in the exterior), all the parallelogram elements in the nth time slab are processed first. This is done in an element-by-element fashion starting from the rightmost element $(n, 1)$ and proceeding to the left of the time slab. The order of processing of elements is clearly shown in Fig. 4. This element-by-element processing is possible because every parallelogram element is contained in the domain of determinacy of its bottom and right edges (see Fig. 4). After all the parallelogram elements in the time slab are processed, we need to obtain a relationship between the field variable and its spatial derivative at the boundary $x = 0$. This is accomplished

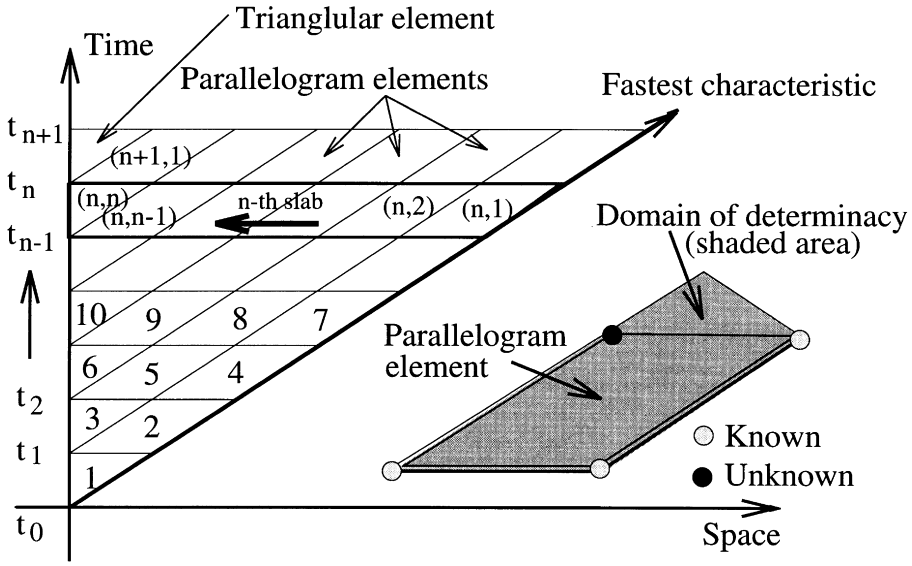

Fig. 4. Domain partitioning for space time Galerkin method.

by solving for the field variable on the triangle (n, n) in a special manner that is consistent with the parallelograms. In the following paragraphs, we explain procedures for both parallelogram and triangular elements.

4.1. Parallelogram element

The type of updating that is performed for the parallelogram element can be viewed as bidirectional stepping, i.e. in space and time simultaneously. The spatial stepping may result in numerical dispersion and the temporal stepping may lead to numerical dissipation. The dispersive properties have an adverse effect on the performance of the method. Because we will be evaluating the traction locally in the triangular element, we require accurate evaluation of the function at the node next to the boundary. However, if dispersion is present, even for a single time step, the value at that node could be completely erroneous. This makes the method extremely sensitive to the type of updating used for the parallelogram element. Initial numerical experiments with space-time discontinuous Galerkin (STDG) methods suggested that the type of updating that they provide results in excessive numerical dissipation (this is similar to the behavior of discontinuous Galerkin methods for first order hyperbolics, Johnson, 1990). For this reason, we resort, at this time, to a continuous Galerkin method.

Cauchy data for second-order hyperbolic systems include both the function value and its normal derivative. This means that the continuous Galerkin method requires C^1 continuity. The basis functions are chosen to be bicubic Hermitian. Use of these functions seems to produce no artificial dispersion. This property can be justified by the non-dissipative behavior of cubic Hermite time-stepping procedures. In what follows, we describe in detail the procedure followed for parallelogram element.

For any given parallelogram element (n,k), we define an affine map taking the parallelogram to a unit square:

$$\bar{x} = \frac{ct - x}{c\Delta t_k} + a_1(n,k), \tag{41}$$

$$\bar{\xi} = \frac{t}{\Delta t_n} + a_2(n,k), \tag{42}$$

where a_1 and a_2 are chosen such that the image of the bottom right corner of the parallelogram is $(0,0)$ in $\bar{x}-\bar{\xi}$ coordinate system. With this transformation, we have the following form for the governing differential equation:

$$\bar{\mathbf{A}}\mathbf{U}_{\bar{x}\bar{x}} + \bar{\mathbf{C}}\mathbf{U}_{\bar{x}\bar{\xi}} + \bar{\mathbf{M}}\mathbf{U}_{\bar{\xi}\bar{\xi}} + (\bar{\mathbf{D}} - \bar{\mathbf{D}}^T)\mathbf{U}_{\bar{x}} + \bar{\mathbf{R}}\mathbf{U} = \mathbf{0}, \tag{43}$$

where

$$\bar{\mathbf{A}} = \frac{1}{\Delta t_k^2}\left(\mathbf{M} - \frac{1}{c^2}\mathbf{A}\right) \tag{44}$$

$$\bar{\mathbf{C}} = \frac{2}{\Delta t_n \Delta t_k}\mathbf{M} \tag{45}$$

$$\bar{\mathbf{M}} = \frac{1}{\Delta t_n^2}\mathbf{M} \tag{46}$$

$$\bar{\mathbf{D}} = \frac{1}{\Delta t_k}\mathbf{D} \tag{47}$$

$$\bar{\mathbf{R}} = \mathbf{R}. \tag{48}$$

As an aside, we note that the matrices $\bar{\mathbf{A}}$, $\bar{\mathbf{C}}$ and $\bar{\mathbf{M}}$ are positive definite and $\bar{\mathbf{R}}$ is positive semi-definite. We do not make use of this property now, but we believe that it may be of key significance to the stability of the space-time method.

The local problem is to solve for the field variable on a unit square $(0,1)\times(0,1)$, with the Cauchy data specified on the bottom and left edges ($\{0\}\times(0,1)$ and $(0,1)\times\{0\}$). As mentioned above, we assume bicubic variation of the field variable on the square, i.e., the function is represented by its values and derivatives $\{\mathbf{U}, \mathbf{U}_{\bar{x}}, \mathbf{U}_{\bar{\xi}}, \mathbf{U}_{\bar{x}\bar{\xi}}\}$ at the four corners:

$$\mathbf{U}(\bar{x},\bar{\xi}) = \sum_{i=1}^{4} N_i(\bar{x},\bar{\xi})\mathbf{U}^i + \sum_{i=1}^{4} N_i^{\bar{x}}(\bar{x},\bar{\xi})\mathbf{U}_{\bar{x}}^i + \sum_{i=1}^{4} N_i^{\bar{\xi}}(\bar{x},\bar{\xi})\mathbf{U}_{\bar{\xi}}^i + \sum_{i=1}^{4} N_i^{\bar{x}\bar{\xi}}(\bar{x},\bar{\xi})\mathbf{U}_{\bar{x}\bar{\xi}}^i. \tag{49}$$

The node numbering for both parallelogram element and for the corresponding master element are shown in Fig. 5. The shape functions in the above equations are given by:

$$\begin{aligned} N_1 &= \psi_1(\bar{x})\psi_1(\bar{\xi}) \quad N_1^{\bar{x}} = \psi_2(\bar{x})\psi_1(\bar{\xi}) \\ N_1^{\bar{\xi}} &= \psi_1(\bar{x})\psi_2(\bar{\xi}) \quad N_1^{\bar{x}\bar{\xi}} = \psi_2(\bar{x})\psi_2(\bar{\xi}), \end{aligned} \tag{50}$$

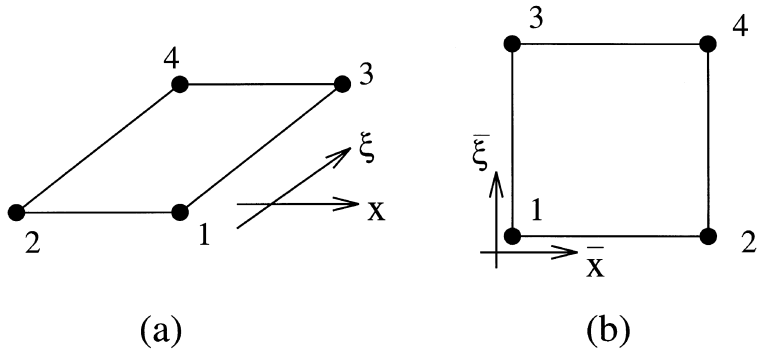

Fig. 5. Node numbering for parallelogram element: (a) actual element; (b) master element.

$$N_2 = \psi_3(\bar{x})\psi_1(\bar{\xi}) \quad N_2^{\bar{x}} = \psi_4(\bar{x})\psi_1(\bar{\xi})$$
$$N_2^{\bar{\xi}} = \psi_3(\bar{x})\psi_2(\bar{\xi}) \quad N_2^{\bar{x}\bar{\xi}} = \psi_4(\bar{x})\psi_2(\bar{\xi}), \tag{51}$$
$$N_3 = \psi_1(\bar{x})\psi_3(\bar{\xi}) \quad N_3^{\bar{x}} = \psi_2(\bar{x})\psi_3(\bar{\xi})$$
$$N_3^{\bar{\xi}} = \psi_1(\bar{x})\psi_4(\bar{\xi}) \quad N_3^{\bar{x}\bar{\xi}} = \psi_2(\bar{x})\psi_4(\bar{\xi}), \tag{52}$$
$$N_4 = \psi_3(\bar{x})\psi_3(\bar{\xi}) \quad N_4^{\bar{x}} = \psi_4(\bar{x})\psi_3(\bar{\xi})$$
$$N_4^{\bar{\xi}} = \psi_3(\bar{x})\psi_4(\bar{\xi}) \quad N_4^{\bar{x}\bar{\xi}} = \psi_4(\bar{x})\psi_4(\bar{\xi}). \tag{53}$$

In the above, ψ_i are the cubic Hermite interpolation functions given by:

$$\psi_1(\alpha) = 2\alpha^3 - 3\alpha^2 + 1 \tag{54}$$
$$\psi_2(\alpha) = \alpha^3 - 2\alpha^2 + \alpha \tag{55}$$
$$\psi_3(\alpha) = -2\alpha^3 + 3\alpha^2 \tag{56}$$
$$\psi_4(\alpha) = \alpha^3 - \alpha^2. \tag{57}$$

We satisfy the differential equation, eqn (43), in a weighted-residual sense. Observations from time stepping schemes imply that when the weight functions are chosen as the shape functions associated with $\mathbf{U}$ and $\mathbf{U}_t$, the weighted residual scheme gives almost no numerical dissipation. Extending this to bidirectional stepping, we chose the weight functions to be the shape functions associated with the unknown degrees of freedom (N_4, $N_4^{\bar{x}}$, $N_4^{\bar{\xi}}$, $N_4^{\bar{x}\bar{\xi}}$), i.e. we have four weight functions and sixteen basis functions and satisfy the weighted residual equation as follows:

$$\int_{\square} w_i Du = 0, \tag{58}$$

where, D is the differential operator in eqn (43). In matrix form, the equation can be written as:

$$\mathbf{K}_{4N\times 16N}\bar{\mathbf{U}}_{16N\times 1} = \mathbf{0}, \tag{59}$$

where, $\bar{\mathbf{U}}$ contains all the nodal degrees of freedom, of which $12N$ are known. Written in a different form, we get

$$\mathbf{K}^u_{4N\times 4N}\bar{\mathbf{U}}^u_{4N\times 1} = \mathbf{K}^k_{4N\times 12N}\bar{\mathbf{U}}^k_{12N\times 1}, \tag{60}$$

where $\bar{\mathbf{U}}^u$ represents the unknown values at the top-left corner of the parallelogram element (node 4) and $\bar{\mathbf{U}}^k$ are the known degrees of freedom at the other three nodes (nodes 1, 2, 3). We notice that, if **A**, **M**, **R** and **D** are block-banded with block size b, $\mathbf{K}^u$ is block banded with $4b$ block size and the block size for $\mathbf{K}^k$ is $12b$. One of the immediate concerns when this procedure is employed is as to whether $\mathbf{K}^u$ is nonsingular or not. Although it is not trivial to prove the invertibility of $\mathbf{K}^u$, by extending the logic from time-stepping procedures, it seems that $\mathbf{K}^u$ is nonsingular provided $\bar{\mathbf{A}}$, $\bar{\mathbf{C}}$ and $\bar{\mathbf{M}}$ are positive definite and $\bar{\mathbf{R}}$ is positive semidefinite and $\bar{\mathbf{D}} = 0$. In cases where $\bar{\mathbf{D}} \neq \mathbf{0}$, we do not have any insight yet as to whether $\mathbf{K}^u$ is always nonsingular or not. However, several numerical experiments indicated that $\mathbf{K}^u$ is nonsingular for all practical purposes. Thus, we have developed a procedure of finding the field variable over a parallelogram element from the required Cauchy data. Furthermore, numerical experiments verified that this method gives no numerical dissipation making it an attractive updating procedure.

4.2. Triangular element

Having established the procedure for the parallelogram element, we can solve for the field variable on all the parallelogram elements in a time slab, when the Cauchy data is given at the previous time point ($t = t_{n-1}$). We now need to process the triangle to get a relation between $\mathbf{U}_x$ and $\mathbf{U}$ at $x = 0$. The straightforward way of doing this is to assume quadratic interpolation between the boundary node (at $x = 0$) and the node next to it (at $x = c\Delta t_n$). This procedure has two inherent pitfalls. First is the property of phase shift arising commonly in extrapolation techniques. More importantly, this process does not give the mixed derivative ($\mathbf{U}_{\bar{x}\bar{\xi}}$) at the boundary node. The mixed derivative is essential for updating the parallelogram $(n+1, n)$. Although it is possible to obtain this by resorting to special tricks of postprocessing, none of the attempted techniques yielded satisfactory performance for practical time-step sizes. For this reason, we opted to satisfy the governing differential equation in the triangular region in a weighted residual sense. The interpolation used in the triangle is chosen so that it conforms with the cubic interpolation of the two adjoining parallelogram elements, $(n, n-1)$ and $(n+1, n)$, and with the time-stepping procedure for the interior. The degrees of freedom are chosen as $\{\mathbf{U}, \mathbf{U}_{\bar{x}}, \mathbf{U}_{\bar{x}\bar{\xi}}\}$ at the boundary node to be solved (node 3 in Fig. 6), an auxiliary degree of freedom (ϕ) and the usual degrees of freedom for the other two nodes (nodes 1, 2 in Fig. 6).

$$\mathbf{U}(\bar{x},\bar{\xi}) = \sum_{i=1}^{3} N_i(\bar{x},\bar{\xi})\mathbf{U}^i + \sum_{i=1}^{3} N_i^{\bar{x}}(\bar{x},\bar{\xi})\mathbf{U}^i_{\bar{x}} + \sum_{i=1}^{2} N_i^{\bar{\xi}}(\bar{x},\bar{\xi})\mathbf{U}^i_{\bar{\xi}} + \sum_{i=1}^{3} N_i^{\bar{x}\bar{\xi}}(\bar{x},\bar{\xi})\mathbf{U}^i_{\bar{x}\bar{\xi}} + N_\phi(\bar{x},\bar{\xi})\phi. \tag{61}$$

In the above, shape functions for the first two nodes are given by:

$$N_1 = \psi_1(\bar{x})\psi_1(\bar{\xi}) \quad N_1^{\bar{x}} = \psi_2(\bar{x})\psi_1(\bar{\xi})$$

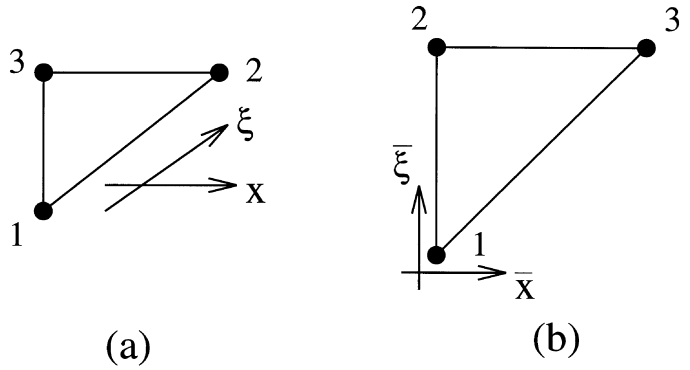

Fig. 6. Node numbering for triangle element: (a) actual element; (b) master element.

$$N_1^{\bar{\xi}} = \psi_1(\bar{x})\psi_2(\bar{\xi}) \quad N_1^{\bar{x}\bar{\xi}} = \psi_2(\bar{x})\psi_2(\bar{\xi}), \tag{62}$$

$$N_2 = \psi_1(\bar{x})\psi_3(\bar{\xi}) \quad N_2^{\bar{x}} = \psi_2(\bar{x})\psi_3(\bar{\xi})$$

$$N_2^{\bar{\xi}} = \psi_1(\bar{x})\psi_4(\bar{\xi}) \quad N_2^{\bar{x}\bar{\xi}} = \psi_2(\bar{x})\psi_4(\bar{\xi}). \tag{63}$$

The shape functions associated with node 3 are:

$$N_3 = \bar{x}^2(1-2\bar{x}\bar{\xi}^2+2\bar{\xi}^3), \tag{64}$$

$$N_3^{\bar{x}} = \bar{x}^2(\bar{x}-\bar{\xi})\bar{\xi}^2, \tag{65}$$

$$N_3^{\bar{x}\bar{\xi}} = \frac{\bar{x}^2(\bar{x}-\bar{\xi})(-3-2\bar{\xi}+5\bar{\xi}^2)}{8}. \tag{66}$$

The interpolation function associated with the auxiliary degree of freedom is a bubble function which enriches the trial function space and renders the functional variation of the displacement similar to that in the parallelogram. This bubble interpolation function is given by:

$$N_\phi(\bar{x},\bar{\xi}) = \bar{x}^2(\bar{\xi}-1)^2(\bar{\xi}-\bar{x}). \tag{67}$$

We note that this function preserves the C^1 continuity of the field variable across the parallelogram-triangle interfaces and is compatible with the time-stepping scheme for the interior.

As in the case of parallelogram elements, we satisfy the differential equation in a weighted residual sense over the triangle. The weight functions are chosen to be the interpolation functions associated with the unknown degrees of freedom ($\{\mathbf{U}, \mathbf{U}_{\bar{x}}, \mathbf{U}_{\bar{x}\bar{\xi}}, \phi\}$). This results in a matrix equation of the following form:

$$\mathbf{K}_{4N\times 4N}\begin{Bmatrix} \mathbf{U} \\ \mathbf{U}_{\bar{x}} \\ \mathbf{U}_{\bar{x}\bar{\xi}} \\ \phi \end{Bmatrix} = \mathbf{R}_{4N\times 1}. \tag{68}$$

In the above equation, **K** is sparse provided that all the coefficient matrices in the governing differential equation are sparse. **K** is, however, not symmetric. The part of **K** corresponding to **U** and $\mathbf{U}_{\bar{x}}$ is coupled with the interior. For this reason, when **K** is not sparse, it is preferable to eliminate the variable $\mathbf{U}_{\bar{x}\bar{\xi}}$ and ϕ at this level. In other cases where **K** is sparse, we include $\mathbf{U}_{\bar{x}\bar{\xi}}$ and ϕ with the matrix problem for the interior. Further properties of **K** that help analyze the stability of the method are not clear due to its complicated structure. However, computations indicate that the method is stable for a wide range of problems. We now go on to the analysis of the computational cost of the above procedure.

5. Computational cost

In the case of constant time step, we obtain all the required matrices before we start the analysis. We then use these matrices for each time step. Also, the matrix $\mathbf{K}^u$ is factorized only once. The matrices in eqn (38) are assumed to be banded $N \times N$ matrices with bandwidth b. The matrix $\mathbf{K}^u$ will then have a bandwidth of $4b$ and $\mathbf{K}^k$ will have $12b$ bandwidth. This means that a single update of a parallelogram element, eqn (60), would take $O(bN)$ flops for both multiplication and solution. And we perform $n^2/2$ updates for n time steps making the total cost of these updates to be $O(bNn^2)$. Because only n triangular updates are performed, the cost of these updates is an order of magnitude lower than that of parallelogram elements. This implies that the total cost for the exterior domain is $O(bNn^2)$. The storage required would be $O(Nb)$ for the matrices and $4Nn$ for the Cauchy data, i.e. the total storage would be approximately $4Nn$. If variable time steps are used, the cost would be much higher and we suggest using few specific time step sizes and storing the corresponding matrices before the analysis.

Both the storage and computation cost for the exterior are much less than the methods based on the Green's function. In those methods, we need to store nN^2 for the Green's function in addition to Nn for the history. The computational cost is kN^2 for the kth time step making the total cost to be $n^2N^2/2$. It is obvious that the STG method is very effective for this part of the computation. However, we note that the current version of the STG method has adverse effects on the solution procedure for the interior.

One obvious question that arises is: how does the STG method compare with other explicit methods? Numerical experiments indicate that the central difference method performs better, provided that we use superconvergent stress recovery technique. It is however observed that the propagation is better modeled by the STG technique than the central difference method. This implies that the performance of the method is degraded by the treatment of the triangular element. A superconvergent traction recovery for this method, if obtained, could solve this problem. Also, numerical experiments indicate that the required time step size for the STG method is larger than the critical time step size for central difference method.

6. Numerical experiments

The performance of the STG method is illustrated with the help of an application to an elastic layer in plane strain. The layer is descretized with one degree of freedom each for horizontal and

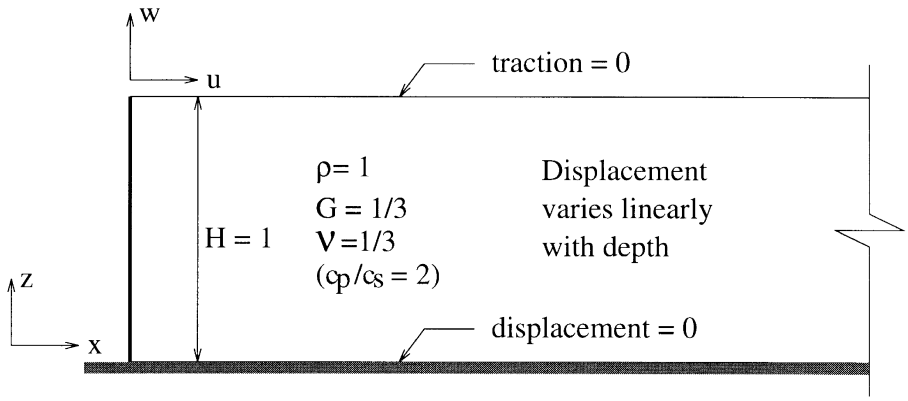

Fig. 7. Numerical example: elastic layer in plane strain.

vertical directions. The displacements are assumed to be linearly varying with depth. The material properties and other relevant details are shown in Fig. 7. For the treatment of the triangular element, the interior time stepping procedure is assumed to be based on constant-average acceleration.

We first carry out the time-harmonic analysis of the above system and obtain the dynamic stiffness matrix in frequency domain. The time step size is assumed to be equal to $(c_{\max}/c_{\min})$ $\min(T, T_0)/6$, where $c_{\max}$ and $c_{\min}$ are the extreme wave speeds, T is the time period of the applied load and T_0 is the cut-off time period. The $c_{\max}/c_{\min}$ factor is chosen such that all the wave phenomena present are modeled accurately. Ignoring this will result in erroneous results (not presented here). In Figs 8 to 11, we compare the results with frequency-domain solution using a hyperelement (same as a consistent transmitting boundary (Tassoulas, 1981). It can be observed that the method is fairly accurate, but has some phase errors at high frequencies. Also, the method seems to smoothen the dynamic stiffness matrix in the frequency domain, i.e. the method supplies some artificial numerical dissipation. Both of these phenomena are associated with the treatment of the triangular element which, at this time seems to be the bottleneck. As expected, the coupling terms in the stiffness matrix (Figs 9 and 10), although close, are not the same. Numerical experiments (not presented here) indicate that the convergence rate for the error in the dynamic stiffness matrix is $O(\Delta t^2)$.

Transient analysis is performed on the same system under a square sine pulse described in Fig. 12. The results are compared with the results from the procedure based on FFT and the hyperelement. The time step size is chosen again as $(c_{\max}/c_{\min})\min(T, T_0)/6$, where T here is the duration of the loading. The displacement is first applied in the horizontal direction and the corresponding forces in horizontal and vertical direction are shown in Figs 13 and 14. The results compare well with the exact solution. Similar comparisons when displacement is applied in the vertical direction can be found in Figs 15 and 16. Note that the error at high frequencies is reflected in the early part of the response when vertical displacement is applied. This is because the proposed method does

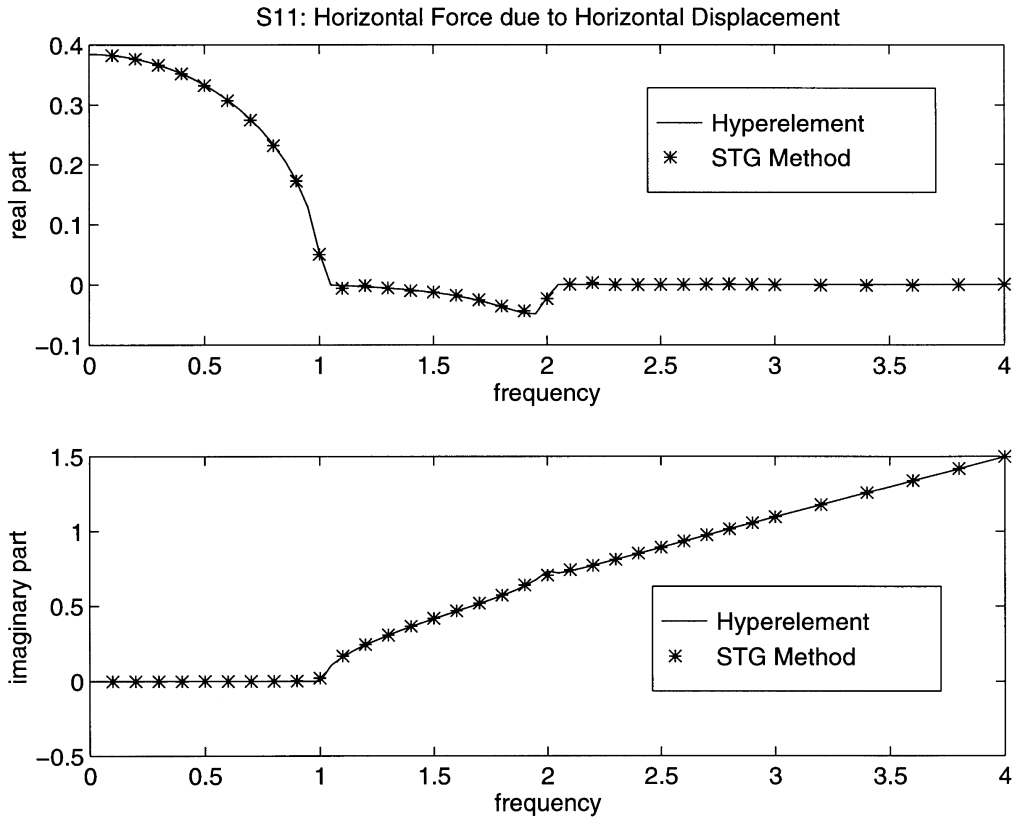

Fig. 8. Comparison of STG solution with the hyperelement in frequency domain: horizontal force due to horizontal displacement.

not model properly the waves with speed lower than the mesh speed (this is also typical of time marching methods (Marfurt, 1984)).

7. Concluding remarks

In this paper, we proposed a space-time Galerkin technique for modeling stratified elastic and acoustic layers. It is an element-by-element computational technique on a space-time mesh and is based on the concept of domain of determinacy. Numerical experiments were presented to illustrate the accuracy of the method. The technique is more economical than the Green's function approach. The current version of the method is more expensive than the central difference method, but the stability properties seem better.

The obvious source of computational cost is the use of higher-order interpolation functions. C^1 continuity imposes restriction on the order of interpolation, and we should resort to discontinuous Galerkin methods to be able to use lower order interpolation. However, at this time, it is not clear as to how the numerical dissipation can be minimized, if not eliminated. It may be possible to

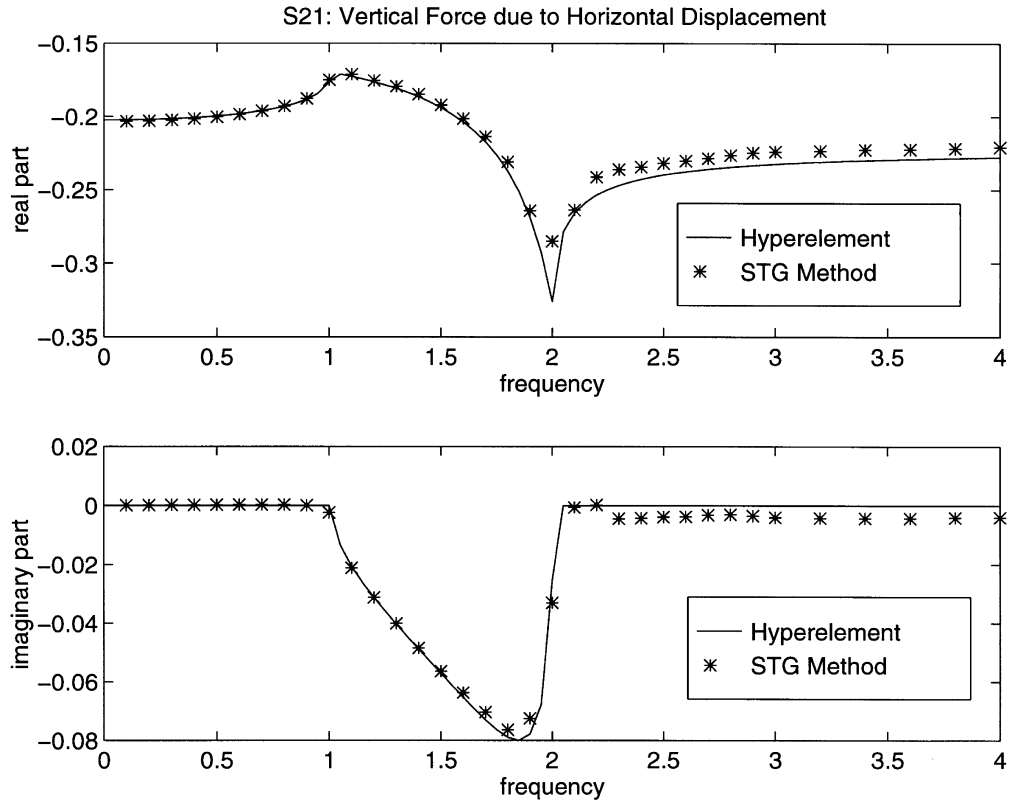

Fig. 9. Comparison of STG solution with the hyperelement in frequency domain: vertical force due to horizontal displacement.

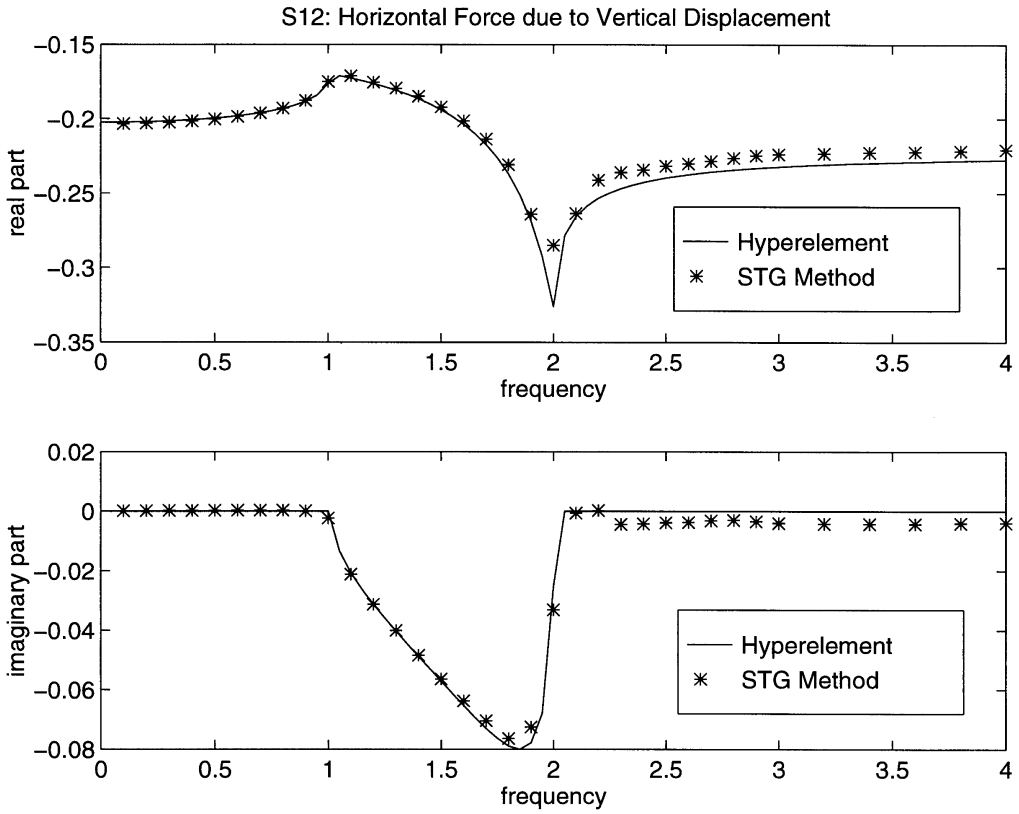

Fig. 10. Comparison of STG solution with the hyperelement in frequency domain: horizontal force due to vertical displacement.

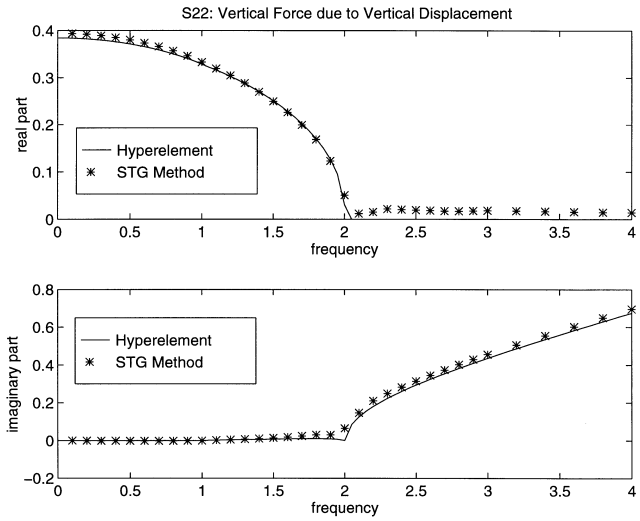

Fig. 11. Comparison of STG solution with the hyperelement in frequency domain: vertical force due to vertical displacement.

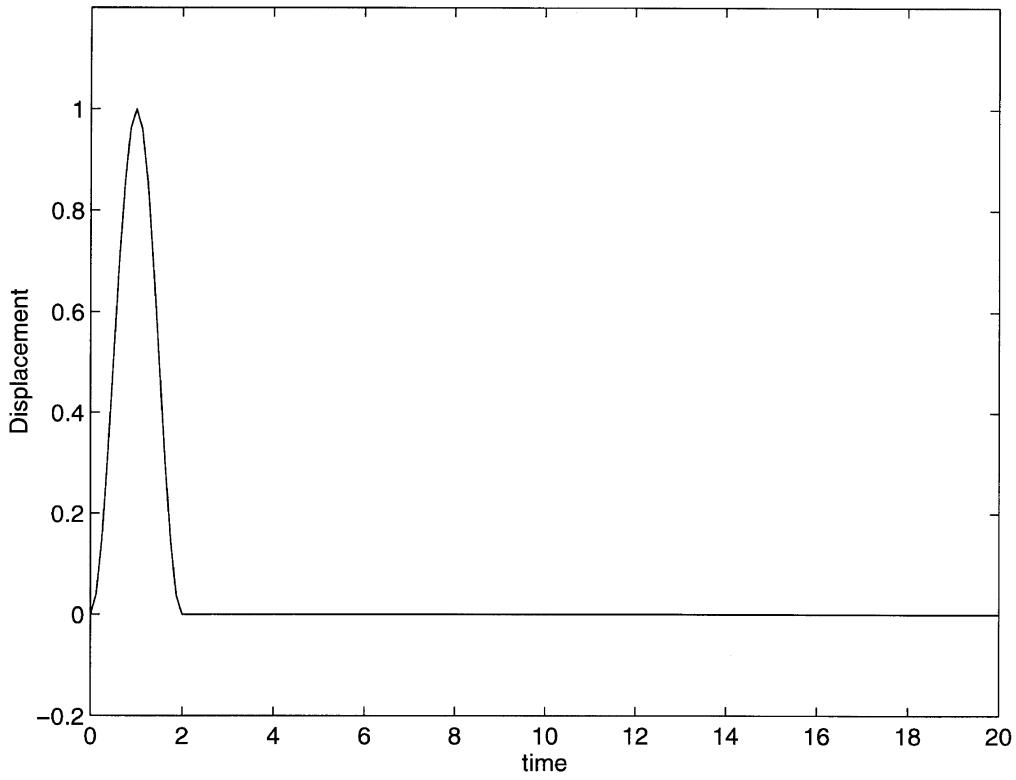

Fig. 12. Displacement loading function used in the transient analyses.

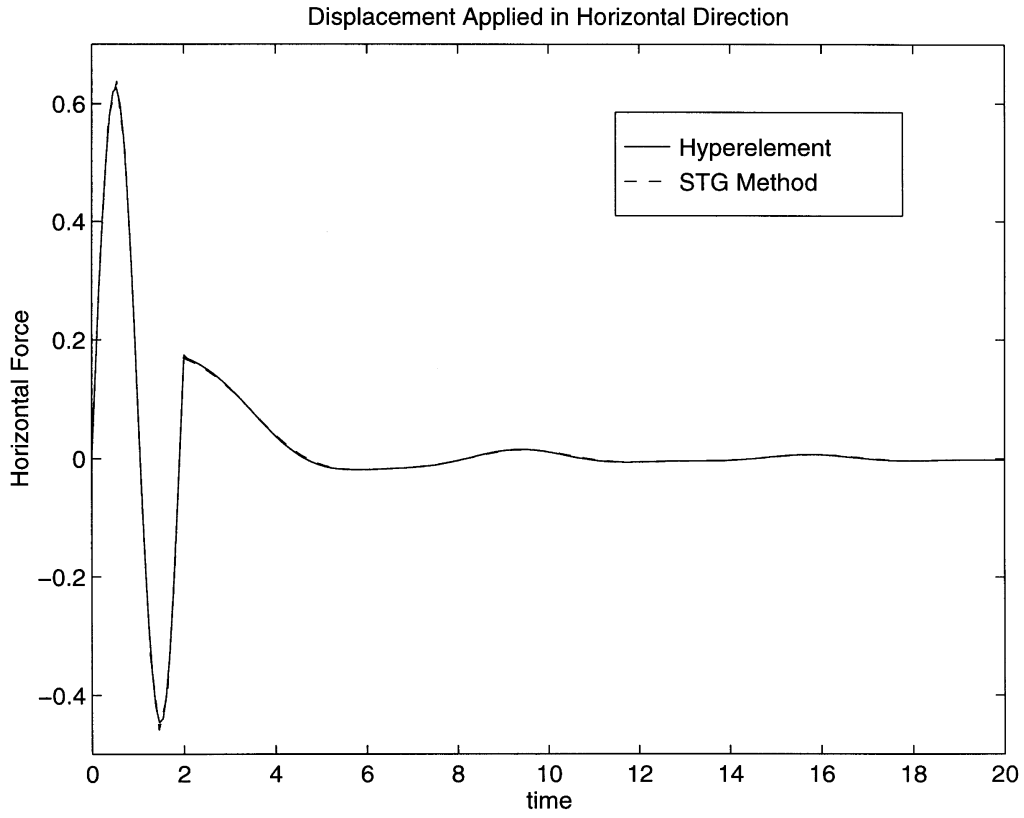

Fig. 13. Comparison of STG solution with the hyperelement in time domain: horizontal force due to horizontal displacement.

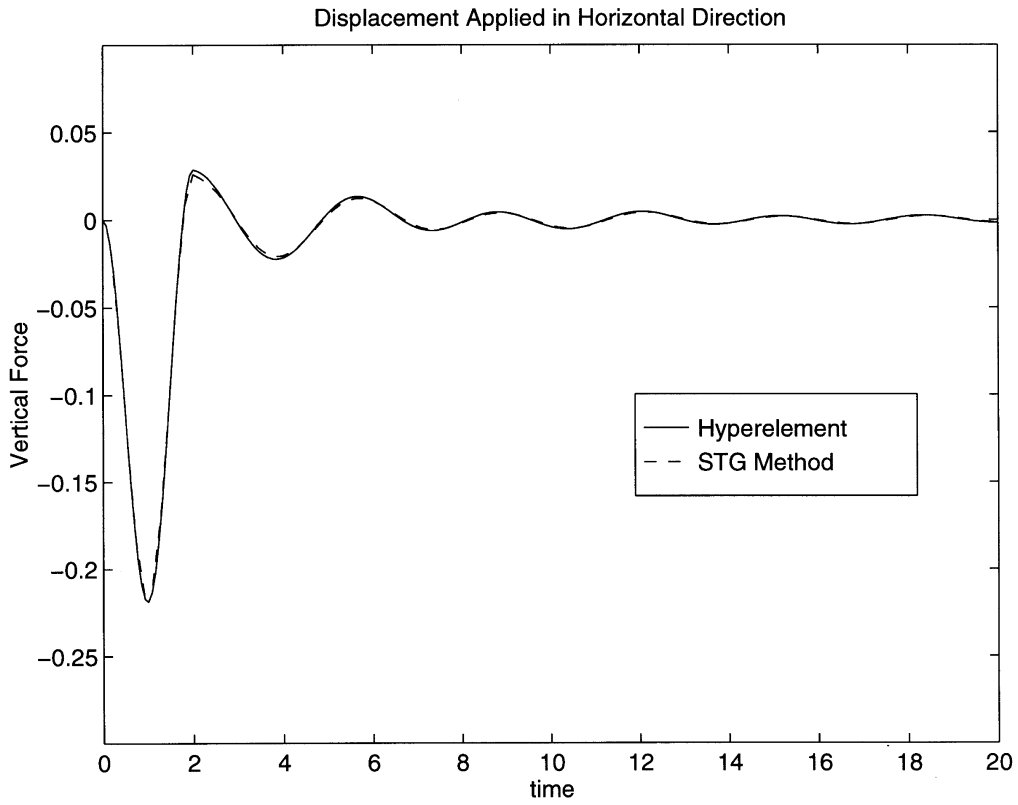

Fig. 14. Comparison of STG solution with the hyperelement in time domain: vertical force due to horizontal displacement.

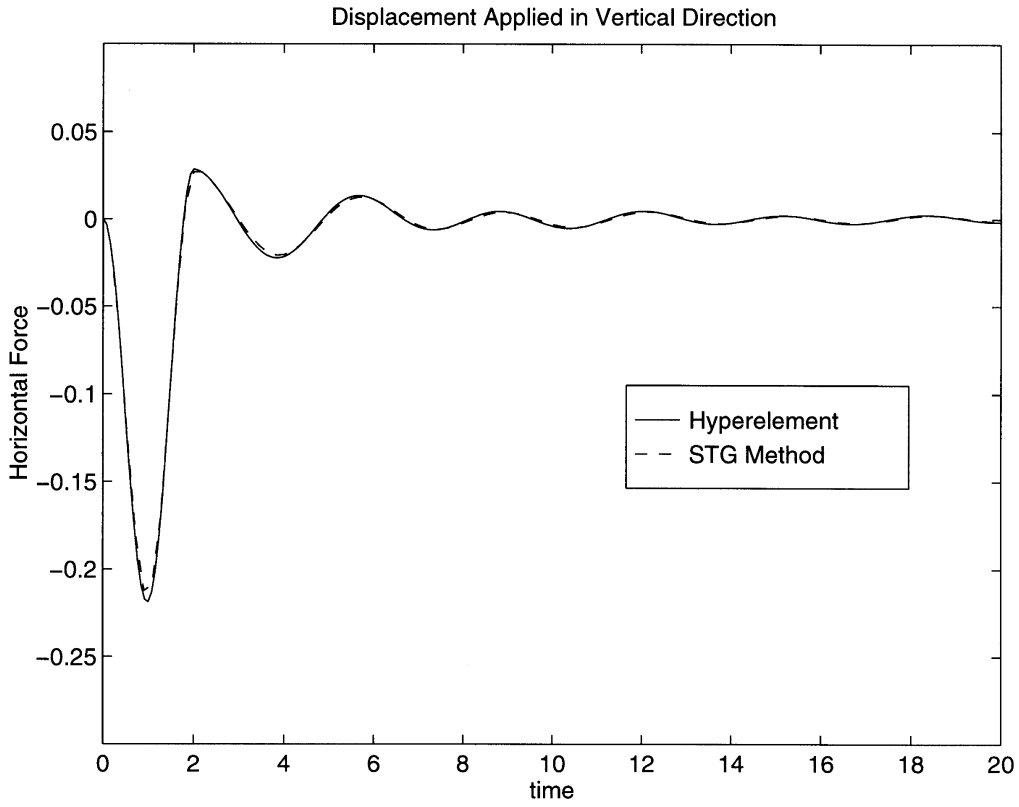

Fig. 15. Comparison of STG solution with the hyperelement in time domain: horizontal force due to vertical displacement.

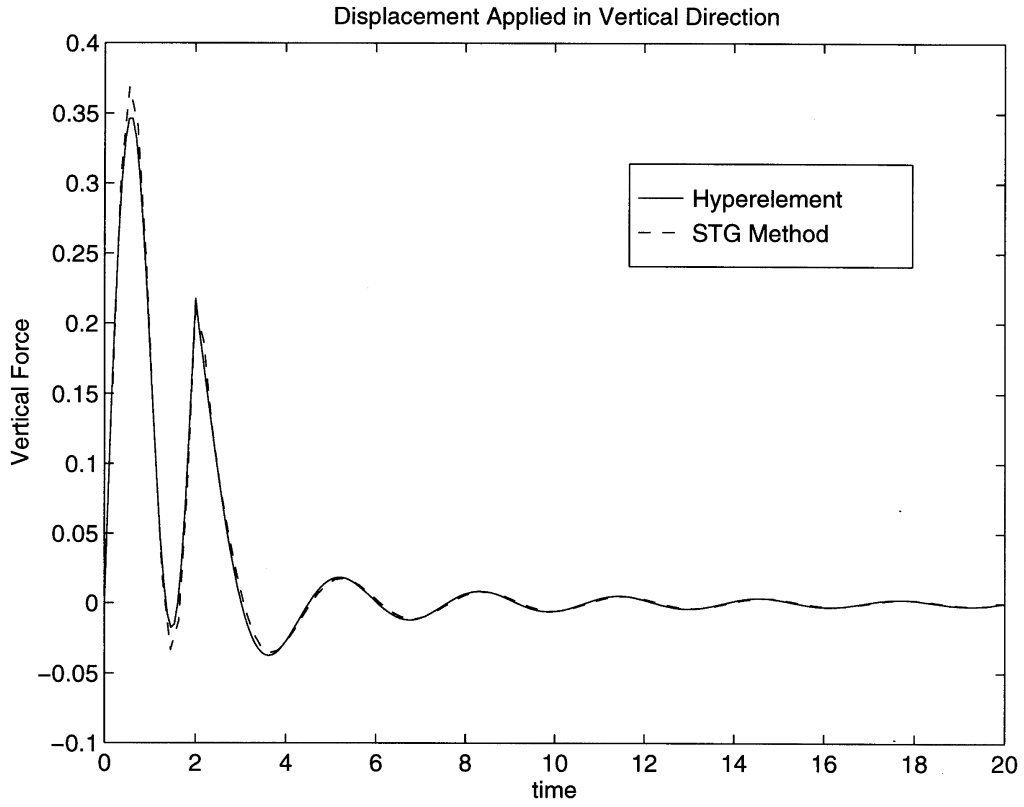

Fig. 16. Comparison of STG solution with the hyperelement in time domain: vertical force due to vertical displacement.

choose an appropriate weight function to accomplish this. Further research will be focused on ways of minimizing the dispersion for the parallelogram element with a discontinuous Galerkin technique.

Another venue for improvement is the treatment of the triangular element. The current treatment of the triangular element results in a stiffness matrix whose properties are not attractive. The possibility of a better treatment of the triangular element is being investigated.

References

Achenbach, J.D., 1973. Wave Propagation in Elastic Solids. North–Holland Publishing Company, Amsterdam.

Bedford, A., Drumheller, D.S., 1994. Introduction to Elastic Wave Propagation. John Wiley and Sons Ltd., Chichester.

Courant, R., Hilbert, D., 1966. Methods of Mathematical Physics, vol. 2. Interscience Publishers, New York.

Dasgupta, G., 1982. A finite element formulation for unbounded homogeneous continua. Journal of Applied Mechanics, ASME 49, 136–140.

Garabedian, P.R., 1964. Partial Differential Equations. John Wiley and Sons, New York.

Givoli, D., 1992. Numerical Methods for Problems in Infinite Domains. Elsevier Science Publishers B.V., Amsterdam.

Guddati, M.N., Tassoulas, J.L., 1997a. An efficient numerical algorithm for transient analysis of exterior wave propagation in a homogeneous layer. Computer Methods in Applied Mechanics and Engineering, submitted for publication.

Guddati, M.N., Tassoulas, J.L., 1997b. Characteristics methods for transient analysis of wave propagation in unbounded domains. Computer Methods in Applied Mechanics and Engineering, in press.

Johnson, C., 1990. Numerical Solution of Partial Differential Equations by the Finite Element Method. Cambridge University Press, Cambridge.

Kausel, E., 1992. Thin-layer method: formulation in the time domain. International Journal for Numerical Methods in Engineering 37, 927–941.

Kausel, E., Roesset, J.M., Waas, G., 1975. Dynamic analysis of footings on layered media. ASCE Journal of Engineering Mechanics 101, 679–693.

Lin, H., Tassoulas, J.L., 1986. A hybrid method for three-dimensional problems of dynamics of foundations. Earthquake Engineering and Structural Dynamics 14, 61–74.

Marfurt, K.J., 1984. Accuracy of finite-difference and finite-element modeling of the scalar and elastic wave equations. Geophysics 49, 533–549.

Roesset, J.M., Scaletti, H., 1979. Boundary matrices for semi-infinite problems. Proceedings of the Third Engineering Mechanics Conference, ASCE, pp. 384–387.

Tassoulas, J.L., 1981. Elements for the numerical analysis of wave propagation in layered media. Research Report R81-2, Department of Civil Engineering. Order No. 689, Massachusetts Institute of Technology, Cambridge, M.A.

Waas, G., 1972. Linear two-dimensional analysis of soil dynamics problems in semi-infinite layered media. Ph.D. dissertation, University of California, Berkeley, CA.

Wolf, J.P., 1988. Soil-Structure Interaction in Time Domain. Prentice–Hall, Englewood Cliffs, NJ.

Wolf, J.P., Song, C., 1996. Finite Element Modeling of Unbounded Media. John Wiley and Sons Ltd., Chichester.